Structural asymmetry in a conserved signaling system that regulates division, replication, and virulence of an intracellular pathogen

Jonathan W. Willett[a,b], Julien Herrou[a,b], Ariane Briegel[c], Grant Rotskoff[a], and Sean Crosson[a,b,d,1]

[a]Department of Biochemistry and Molecular Biology, University of Chicago, Chicago, IL 60637; [b]Howard Taylor Ricketts Laboratory, University of Chicago, Argonne National Laboratory, Argonne, IL 60439; [c]Division of Biology and Biological Engineering, California Institute of Technology, Pasadena, CA 91125; and [d]The Committee on Microbiology, University of Chicago, Chicago, IL 60637

Edited by Graham C. Walker, Massachusetts Institute of Technology, Cambridge, MA, and approved June 2, 2015 (received for review February 13, 2015)

We have functionally and structurally defined an essential protein phosphorelay that regulates expression of genes required for growth, division, and intracellular survival of the global zoonotic pathogen *Brucella abortus*. Our study delineates phosphoryl transfer through this molecular pathway, which initiates from the sensor kinase CckA and proceeds through the ChpT phosphotransferase to two regulatory substrates: CtrA and CpdR. Genetic perturbation of this system results in defects in cell growth and division site selection, and a specific viability deficit inside human phagocytic cells. Thus, proper control of *B. abortus* division site polarity is necessary for survival in the intracellular niche. We further define the structural foundations of signaling from the central phosphotransferase, ChpT, to its response regulator substrate, CtrA, and provide evidence that there are at least two modes of interaction between ChpT and CtrA, only one of which is competent to catalyze phosphoryltransfer. The structure and dynamics of the active site on each side of the ChpT homodimer are distinct, supporting a model in which quaternary structure of the 2:2 ChpT–CtrA complex enforces an asymmetric mechanism of phosphoryl transfer between ChpT and CtrA. Our study provides mechanistic understanding, from the cellular to the atomic scale, of a conserved transcriptional regulatory system that controls the cellular and infection biology of *B. abortus*. More generally, our results provide insight into the structural basis of two-component signal transduction, which is broadly conserved in bacteria, plants, and fungi.

Brucella abortus | two-component system | cell cycle | ChpT | CtrA

Brucellosis, caused by *Brucella* spp., is among the most common zoonotic diseases worldwide (1). These intracellular pathogens are estimated to cause at least 500,000 new human infections each year and, in areas of Africa, Asia, and South America, inflict significant agricultural losses due to decreased livestock production (2, 3). Survival of *Brucella* within mammals is linked to their ability to infect and survive inside professional phagocytic cells (2). If left untreated in human hosts, *Brucella* eventually spread to multiple tissue types, which can lead to a range of debilitating chronic sequelae including reticuloendothelial, cardiovascular, gastrointestinal, and neurological damage.

Brucella are members of the α-proteobacteria, a diverse class of Gram-negative species adapted for growth across a range of environmental conditions including plant surfaces and roots, aquatic and soil ecosystems, and the interior of mammalian cells (4, 5). Among the central regulatory systems controlling the α-proteobacterial cell cycle is a multistep phosphorelay composed of four proteins: (*i*) the hybrid sensor histidine kinase (HK) CckA, (*ii*) the histidine phosphotransferase ChpT, (*iii*) the DNA-binding response regulator CtrA, and (*iv*) the phospho-receiver protein CpdR (Fig. 1). Our current understanding of this conserved regulatory system is based largely on studies of the related aquatic bacterium *Caulobacter crescentus* (6, 7). In *Caulobacter*, autophosphorylated CckA transfers phosphoryl groups to a conserved histidine on ChpT. ChpT~P subsequently transfers phosphoryl groups to either CpdR or CtrA (8). CtrA is a regulator of cell cycle and developmental gene transcription; its activity is controlled by phosphorylation and by proteolysis. Specifically, CtrA is active as a transcription factor when phosphorylated (CtrA~P); CtrA protein is stabilized in the cell by CpdR~P and is proteolyzed when CpdR is in its unphosphorylated form (9). Thus, ChpT regulates CtrA-dependent transcription both by phosphorylating CtrA and controlling CtrA protein stability via CpdR.

The genes encoding the CckA–ChpT–CtrA–CpdR regulatory system have been identified in several α-proteobacteria. However, there is notable diversity in the transcriptional output of this system across the clade (10–13), which likely reflects the breadth of niches inhabited by these species (14). The function of this system in *Brucella abortus*, which is capable of infecting, growing, and replicating inside mammalian cells, is poorly understood, although previous studies of *Brucella* CtrA have revealed a possible role in the control of cell division (15). It is further known that genetic perturbation of the DNA methyltransferase CcrM, which is directly regulated by CtrA, results in a virulence defect (16).

In this study, we define the full set of genes encoding the *B. abortus* CckA–ChpT–CtrA–CpdR phosphorelay and characterize molecular and structural requirements of signaling through this conserved pathway. These four proteins comprise an essential phosphorelay that controls *B. abortus* cell growth, division, and infection biology. Expression of conditional mutant alleles of these

Significance

***Brucella abortus* is an intracellular bacterial pathogen that inflicts a significant health burden on both humans and their livestock on a global scale. We demonstrate that an essential regulatory system controls the growth and morphology of *B. abortus*, and that this system is required for survival inside mammalian host cells. Using experimental and computational tools of structural biology, we further define how the protein components of this regulatory pathway interact at the atomic scale. Our results provide evidence for multiple, asymmetric modes of binding between essential pathway proteins that control transcription. The multimodal molecular interactions we observe provide evidence for new layers of allosteric control of this conserved gene regulatory system.**

Author contributions: J.W.W. and S.C. designed research; J.W.W., J.H., A.B., and G.R. performed research; J.W.W., J.H., A.B., G.R., and S.C. contributed new reagents/analytic tools; J.W.W., J.H., A.B., G.R., and S.C. analyzed data; and J.W.W. and S.C. wrote the paper.

The authors declare no conflict of interest.

This article is a PNAS Direct Submission.

Data deposition: Crystallography, atomic coordinates, and structure factors have been deposited in the Protein Data Bank, www.pdb.org (PDB ID codes 4QPK and 4QPJ).

[1]To whom correspondence should be addressed. Email: scrosson@uchicago.edu.

This article contains supporting information online at www.pnas.org/lookup/suppl/doi:10.1073/pnas.1503118112/-/DCSupplemental.

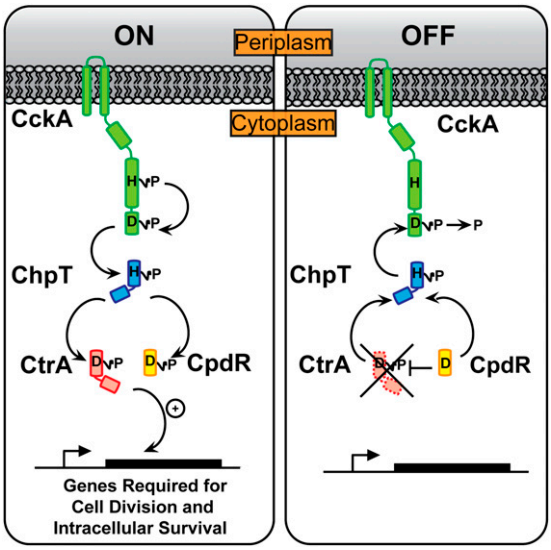

Fig. 1. Model of the CckA–ChpT–CtrA–CpdR phosphorelay. The HK CckA (green) autophosphorylates on a conserved His (H) residue and transfers a phosphoryl group to a conserved Asp (D) residue on its C-terminal REC domain. CckA~P transfers phosphoryl groups to the ChpT phosphotransferase (blue), which can subsequently transfer phosphoryl groups to the REC domains of CtrA (red) and CpdR (yellow). CtrA~P is a DNA-binding response regulator that modulates transcription of genes controlling cell polarity, division, and intracellular survival in mammalian macrophages. CpdR controls steady-state levels of CtrA in the *B. abortus* cell.

genes results in defects in growth and division site selection, yielding cells with branched morphology and altered DNA content. Although genetic perturbation of this pathway has no effect on cell survival in vitro, or entry during a macrophage infection, pathway mutants exhibit significantly reduced survival inside human cells. These data support a model in which the CckA–ChpT–CtrA–CpdR proteins constitute a regulatory system that controls *B. abortus* cell development and intracellular survival. We have further extended our functional analysis of this regulatory system to the molecular scale and determined the structures of *B. abortus* ChpT to 1.7-Å resolution and ChpT bound to the receiver domain of CtrA (ChpT–$CtrA_{REC}$) to 2.7-Å resolution. The ChpT structure reveals a symmetrical homodimer with an HK-like fold. Unlike classic HKs, ChpT does not bind ATP but efficiently and specifically transfers phosphoryl groups from the CckA kinase to the receiver domains of both CtrA and CpdR. The ChpT–$CtrA_{REC}$ crystal structure reveals an asymmetric protein complex that defines a phosphotransferase-receiver interface in molecular detail and provides insight into the mechanism by which ChpT regulates CtrA activity. Our study illuminates, on multiple scales, mechanisms by which a conserved signaling pathway controls the developmental and infection biology of a bacterial intracellular pathogen.

Results

***B. abortus* CckA–ChpT–CtrA–CpdR Constitute a Specific Phosphorelay.** We used sequence-based approaches via the MiST2 database (17) to identify putative orthologs of CckA, ChpT, CtrA, and CpdR in *B. abortus*. Amino acid sequence identity of the putative CckA (Bab1_1059; 65%), ChpT (Bab1_1613; 36%), CtrA (Bab1_1614; 81%), and CpdR (Bab2_0042; 74%) proteins to the *C. crescentus* orthologs (Fig. S1) suggested that *B. abortus* encodes a fully intact CckA–ChpT–CtrA–CpdR phosphorelay. However, overall sequence identity of *B. abortus* Bab1_1613 to bona fide ChpT proteins of other α-proteobacteria was low and did not clearly distinguish Bab1_1613 as a ChpT ortholog. To test our prediction that these four genes constitute a unified signaling pathway in *B. abortus*, we expressed and purified each of these proteins. *B. abortus* CckA (Bab1_1059) is predicted to contain a transmembrane domain at its N terminus, so we generated a construct to express a soluble CckA fragment (amino acids 554–946) that contains only the HK and C-terminal receiver (REC) domains. This truncated CckA yielded an active kinase capable of autophosphorylation in the presence of excess ATP (Fig. 2*A*). Half-maximal autophosphorylation was observed within 5 min; signal for phospho-CckA (CckA~P) saturated within 30 min (Fig. 2*A*) and is consistent with the autophosphorylation profile of other bacterial HKs (18–20).

To test whether *B. abortus* CckA~P transfers a phosphoryl group to the predicted ChpT protein (Bab1_1613), we incubated CckA~P with ChpT for periods of 1–30 min. A clear ChpT~P band appeared within 1 min (Fig. 2*B*). The in vitro phosphotransfer kinetics provides evidence that CckA and ChpT form a cognate signaling interaction in vivo (21). We next sought to identify other possible phosphorylation substrates of CckA~P using the approach known as phosphotransfer profiling (22). Because REC domains are the preferred substrates for bacterial HKs (23), we generated constructs to express the soluble REC domains from each of the 23 response regulator proteins encoded within the *B. abortus* genome. Incubation of CckA~P with each REC domain for 15 s showed no evidence of phosphotransfer (Fig. 2*C*). However, the addition of ChpT to each of these 23 phosphotransfer reactions resulted in rapid phosphorylation of two substrates: CpdR and CtrA. We conclude that phosphotransfer from *B. abortus* CckA to the REC domains of CpdR and CtrA is specific and requires the ChpT protein. Our results provide biochemical support for our prediction that these *B. abortus* genes constitute a bona fide regulatory phosphorelay, and that this gene set is orthologous to

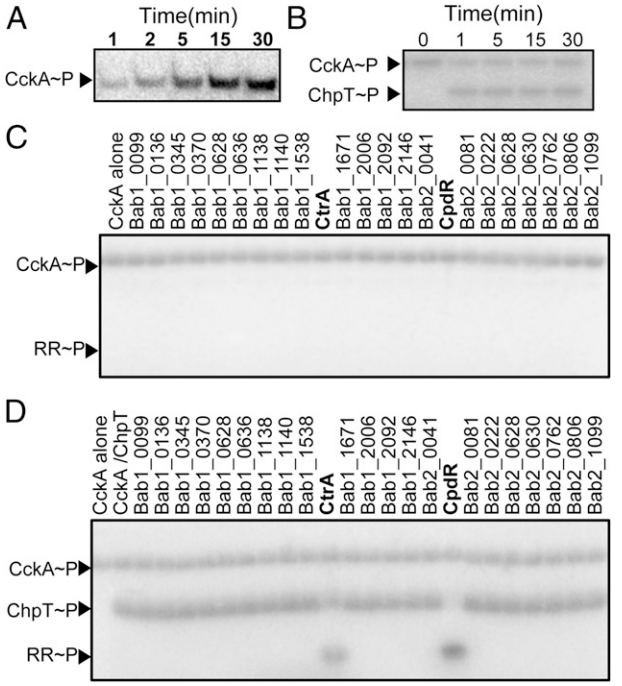

Fig. 2. CckA–ChpT–CtrA–CpdR proteins constitute a phosphorelay system in vitro. (*A*) Autoradiograph of CckA autophosphorylation from 1 to 30 min in the presence of [γ-^{32}P]ATP. (*B*) Autoradiograph of phosphotransfer from CckA~P to ChpT measured from 0 to 30 min in the presence of [γ-^{32}P]ATP. CckA was permitted to autophosphorylate for 30 min before incubation with ChpT. (*C* and *D*) Phosphoryl transfer from CckA~P was assayed for 15 s against all 23 *B. abortus* response regulators in the (*C*) absence or (*D*) presence of ChpT.

the *cckA–chpT–cpdR–ctrA* systems defined in related α-proteobacteria (8, 22).

Genes Encoding CckA–ChpT–CtrA–CpdR Phosphorelay Control *B. abortus* Cell Division. To investigate the function of the CckA–ChpT–CtrA–CpdR phosphorelay in vivo we attempted to delete these genes from their chromosomal loci in *B. abortus*. We were unable to delete or disrupt *cckA*, *chpT*, or *ctrA*, but were able to generate a strain harboring a chromosomal in-frame deletion of *cpdR*. We could only delete the chromosomal copies of *chpT* or *cckA* when expressing a complementing copy of these genes *in trans* from their native promoters (Table S1). Because CckA and ChpT are required to phosphorylate CtrA in vitro (Fig. 2), our inability to delete these genes in the absence of a complementing copy is consistent with previous reports that CtrA is essential in *B. abortus* (15) and several other α-proteobacteria (24–27). Thus, our data provide evidence that the CckA–ChpT–CtrA phosphorelay is essential in *B. abortus*. To further test the effects of phosphorelay perturbation on *B. abortus* biology we generated strains encoding conditional alleles of these genes, which we discuss below.

We first constructed a *B. abortus* strain in which the WT copy of *ctrA* was replaced with the *ctrA(V148F)* allele, a known temperature-sensitive allele of *C. crescentus ctrA* (28). We reasoned this analogous substitution in *B. abortus* CtrA would confer a similar temperature-sensitive phenotype given the high sequence similarity between these proteins (81%) (Fig. S1). Indeed, *B. abortus* expressing *ctrA(V148F)* from the native *ctrA* locus displays no growth defect at 30 °C but fails to replicate when grown at 37 °C (see Fig. 4*D*). Because we could not generate a *B. abortus chpT* null mutant, we sought to disrupt signaling through the CckA–ChpT–CtrA–CpdR pathway by transforming *B. abortus* with an inducible *chpT* overexpression plasmid ($chpT^{++}$). Given that unphosphorylated CpdR regulates steady-state CtrA levels in other α-proteobacteria (9, 29), we also generated strains carrying either WT *cpdR* [$cpdR(WT)^{++}$] or an allele of *cpdR* that cannot be phosphorylated [$cpdR(D52A)^{++}$], which we expressed from a *lac*-inducible promoter on a replicating plasmid.

To assess the effects of expressing these conditional alleles, we cultured WT and mutant *B. abortus* strains to midlogarithmic phase and analyzed cell morphology by cryo-electron microscopy (cryoEM) and light microscopy (LM). WT *B. abortus* cells grown to log phase in complex medium clearly occupied multiple stages of the cell cycle and exhibited hallmarks of cell growth and division described for the order Rhizobiales of α-proteobacteria (30). Specifically, predivisional *B. abortus* cells exhibit features of polar cell growth in which a narrower, rod-shaped cell emerges from the pole of a wider, rounder cell (Fig. 3*A*). In contrast, *ctrA (V148F)* mutant cells cultured for either 4 or 24 h at the nonpermissive temperature (37 °C) were abnormally elongated; by 24 h we observed defects in cell divison, with apparent budding

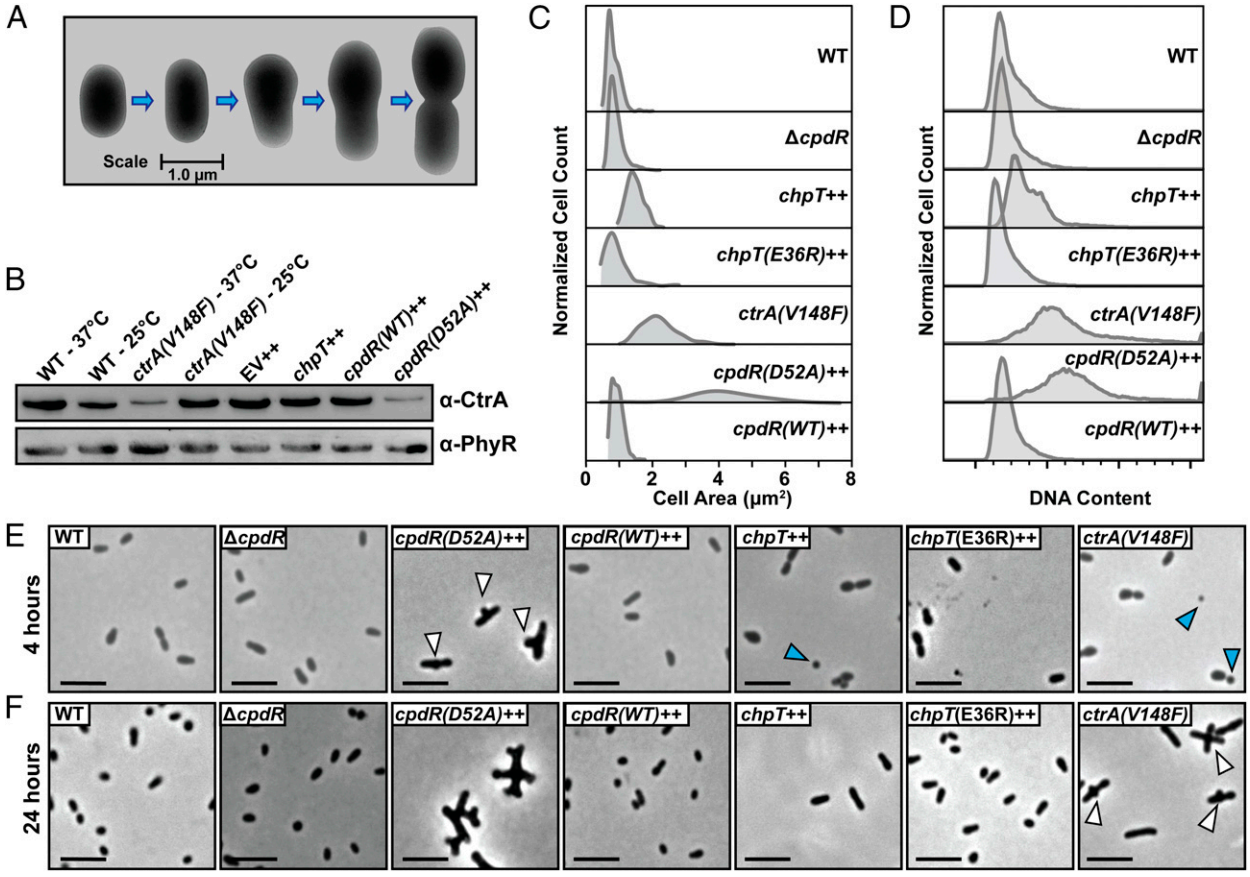

Fig. 3. The CckA–ChpT–CtrA–CpdR phosphorelay regulates *B. abortus* cell division. (*A*) CryoEM images of fixed WT *B. abortus* cells captured at stages through a typical cell cycle. (*B*) Western blot showing steady-state CtrA protein levels 24 h after shift to the nonpermissive temperature [37 °C for *ctrA*(V148F)] or addition of IPTG [*chpT*++, *cpdR*(WT)++, and *cpdR*(D52A)++]. (*C*) Total cell area distributions of populations of *B. abortus* cells ($n \approx 300$) after growth for 24 h under conditions in which conditional alleles are induced/activated. (*D*) DNA content of WT and mutant *B. abortus* cells ($n = 20{,}000$) measured by propidium iodide staining followed by flow cytometry. Light micrographs of WT and mutant *B. abortus* strains taken after (*E*) 4-h and (*F*) 24-h cultivation in complex medium at 37 °C, containing IPTG. Blue arrows mark apparent *B. abortus* minicells; white arrows mark cells with disrupted cell growth and division polarity. (Scale bars, 2 μm.)

from the midcell position (Fig. 3 *E* and *F* and Fig. S2*A*). CtrA (V148F) protein is still present in the cell after growth at 37 °C for 24 h, although at slightly decreased levels (Fig. 3*B*). Induction of *chpT* expression (*chpT*$^{++}$) by the addition of isopropyl β-D-1-thiogalactopyranoside (IPTG) for 4 and 24 h increased the proportion of elongated cells; we further observed the presence of minicells in these cultures (Fig. 3 *E* and *F* and Fig. S2*B*).

Finally, we measured the effects of *cpdR* allele expression on *B. abortus* cell morphology and on steady-state CtrA levels. Because unphosphorylated CpdR activates proteolysis of CtrA in *C. crescentus* (29), we tested whether unphosphorylated CpdR affects steady-state levels of CtrA in *B. abortus.* After inducing *cpdR (WT)*$^{++}$ or *cpdR(D52A)*$^{++}$ expression with IPTG for 24 h, we observed a significant reduction in CtrA protein in the strain expressing *cpdR(D52A)*$^{++}$, which is missing the site of aspartyl phosphorylation. Expression of *cpdR(WT)*$^{++}$ had no effect on steady-state CtrA levels assessed by Western blot (Fig. 3*B*). This result is consistent with a model in which unphosphorylated CpdR destabilizes CtrA in *B. abortus*. We further analyzed *cpdR(WT)*$^{++}$ and *cpdR(D52A)*$^{++}$ overexpression strains by cryoEM and LM and observed large elongated cells with apparent budding at the midcell after 4 h of *cpdR(D52A)*$^{++}$ induction (Fig. 3*E*); after 24 h of induction we observed large *B. abortus* cells that were highly branched, which is consistent with a defect in proper cell division (Fig. 3*F* and Fig. S2). Overexpression of *cpdR(WT)*$^{++}$ or deletion of *cpdR* (Δ*cpdR*) did not result in a gross defect in cell morphology (Fig. 3).

CryoEM and LM images of a small number of cells provide evidence that perturbation of the CckA–ChpT–CtrA–CpdR pathway affects cell growth and division. We next imaged a large number of fixed WT and mutant *B. abortus* cells, extracted the 2D cell contours, and analyzed these cell contours to determine 2D cell area (31). This analysis permitted us to more thoroughly quantify variation in cell area across all strains. After 24 h of growth at 37 °C in complex medium (adding IPTG where applicable) the mean cell area of WT *B. abortus* was 0.67 ± 0.19 μm^2. However, mean cell areas of *ctrA(V148F)* (2.1 ± 0.57 μm^2), *chpT*$^{++}$ (1.1 ± 0.26 μm^2), and *cpdR(D52A)*$^{++}$ (3.9 ± 1.4 μm^2) were significantly increased (one-way ANOVA; Dunnett's post test; $P < 0.0001$) compared with WT. The Δ*cpdR* (0.75 ± 0.22 μm^2) and *cpdR(WT)*$^{++}$ (0.79 ± 0.19 μm^2) strains exhibited less increase in cell area relative to WT but were still significantly larger than WT ($P < 0.001$). We further tested whether the DNA content of these mutant strains differed from WT *B. abortus* by staining DNA with propidium iodide and analyzing DNA content using flow cytometry. The *ctrA(V148F)*, *chpT*$^{++}$, and *cpdR(D52A)*$^{++}$ strains all have highly increased DNA content relative to WT (Fig. 3*D*), consistent with the gross cell division defects of these mutants.

To assess the impact that CckA–ChpT–CtrA–CpdR pathway perturbation has on CtrA-dependent transcription, we quantified transcript levels of the CtrA-regulated gene *ccrM* (15), by quantitative reverse-transcription PCR (qRT-PCR). After 4 h of growth at the nonpermissive temperature or addition of IPTG, *ctrA (V148F)*, *chpT*$^{++}$, and *cpdR(D52A)*$^{++}$ strains have significantly decreased *ccrM* transcript abundance compared with WT *B. abortus* or an empty vector control (Fig. S3). We conclude that these genetic perturbations reduce CtrA-dependent transcription in *B. abortus*. Overall, our data support a model in which phosphorelay through the CckA–ChpT–CtrA–CpdR pathway regulates *B. abortus* processes that determine cell growth, cell cycle, and cell division via control of CtrA-dependent transcription.

The CckA–ChpT–CtrA–CpdR Pathway Is Required for Intracellular Survival of *B. abortus* in Human Macrophages. A natural niche of *B. abortus* is the interior of mammalian cells. We assessed the effect CckA–ChpT–CtrA–CpdR pathway perturbation has on entry, replication, and survival inside terminally differentiated THP-1 macrophages. Before infection, overnight cultures of WT and conditional *B. abortus* mutant strains were grown under noninducing conditions in rich medium. Conditional alleles were then activated/induced by culturing for 4 h at 37 °C with IPTG (where indicated) before infecting macrophages. WT and mutant *B. abortus* cells were added to THP-1 cells at a multiplicity of infection (MOI) of 100 cfu per macrophage. The initial 1 h post infection (hpi) time point in these experiments generally reflects *B. abortus* entry. No statistically significant differences were observed at this time point, indicating there is no defect in macrophage entry of any mutant strain (Fig. 4 *A*–*C*). In contrast, there is a significant reduction in intracellular *B. abortus* replication and/or survival in the *ctrA(V148F)*, *chpT*$^{++}$, and *cpdR(D52A)*$^{++}$ strains relative to WT and uninduced controls at 48 hpi. The number of *ctrA(V148F)* cells isolated from THP-1 (at 37 °C) is ∼1 log lower at 24 hpi and 3.5 logs lower than WT *B. abortus* at 48 hpi (Fig. 4*A*). *ctrA(V148F)* infections performed at the permissive temperature (30 °C) revealed no significant decrease in cfu at 48 hpi compared with WT cultured under equivalent conditions. Overexpression of *chpT*$^{++}$ resulted in a 1.0 log decrease in the number of cells recovered from THP-1 compared with uninduced and empty vector controls at 48 hpi (Fig. 4*B*). The most severe intracellular defect was observed in the strain overexpressing *cpdR(D52A)*$^{++}$: We observed a 1.5 log decrease in cells recovered from THP-1 at 24 hpi and a 3.5 log reduction of recovered cells at 48 hpi relative to the uninduced control. There was no difference in recovery of *B. abortus* expressing *cpdR(WT)*$^{++}$ or the Δ*cpdR* in-frame deletion strain relative to WT (Fig. 4).

We next tested whether mutant attenuation observed in macrophages is due to a general loss of *B. abortus* viability, or whether CckA–ChpT–CtrA–CpdR pathway perturbation results in a replication/survival defect that is specific to the intracellular niche. We first cultured *B. abortus ctrA(V148F)*, *chpT*$^{++}$, and *cpdR (D52A)*$^{++}$ conditional mutants under noninducing conditions in liquid growth medium for 8 h, enumerating bacteria over this growth period. At 8 h (or 1 × 10^7 cfu/mL) we shifted to the restrictive temperature (37 °C) and induced expression of conditional alleles with IPTG; we chose to shift cells at this point because this was the approximate density of cells used for macrophage infections. We enumerated cfu of these induced/activated *B. abortus* mutants at similar time points assayed in our THP-1 macrophage infection experiments (ref. 24, 48 h). Upon induction/activation, the *ctrA(V148F)* and *cpdR(D52A)*$^{++}$ mutants were completely inhibited in replication whereas the *chpT*$^{++}$ mutant replicated, but at a lower rate than WT. In contrast to what we observed in macrophages, neither the *ctrA(V148F)*, *chpT*$^{++}$, nor *cpdR(D52A)*$^{++}$ strains lost viability under these conditions (over 48 h) (Fig. 4*D*). We conclude the reduced numbers of *ctrA(V148F)*, *chpT*$^{++}$, and *cpdR(D52A)*$^{++}$ cells recovered from THP-1 reflects a specific requirement for the CckA–ChpT–CtrA–CpdR pathway for survival inside macrophages. We further conclude that this signaling pathway does not generally control features of the cell required for *B. abortus* entry into mammalian macrophages.

ChpT: A Histidine Phosphotransferase with an HK-Like Structure. Having established the importance of the CckA–ChpT–CtrA–CpdR system in *B. abortus* cellular and infection biology, we next sought to characterize the structural basis of phosphotransfer through this conserved pathway. To this end, we purified, crystallized, and solved the structure of the ChpT phosphotransferase (PDB ID code 4QPK). ChpT formed tetragonal crystals of space group $P4_3$ (a = b = 70.84, c = 87.01 Å) that diffracted to 1.7-Å resolution; we phased the ChpT crystal structure by molecular replacement using a model based on structures of a *C. crescentus* homolog (32, 33). *B. abortus* ChpT was refined to R_{work} = 0.164 and R_{free} = 0.188. Crystallographic data and refinement statistics are summarized in Table S2.

The crystallographic asymmetric unit contains two ChpT molecules, organized as a symmetric dimer. The structure is similar to HKs (34–36) and other histidine phosphotransfer (Hpt) proteins (32, 33, 37). Each ChpT monomer is composed of an N-terminal

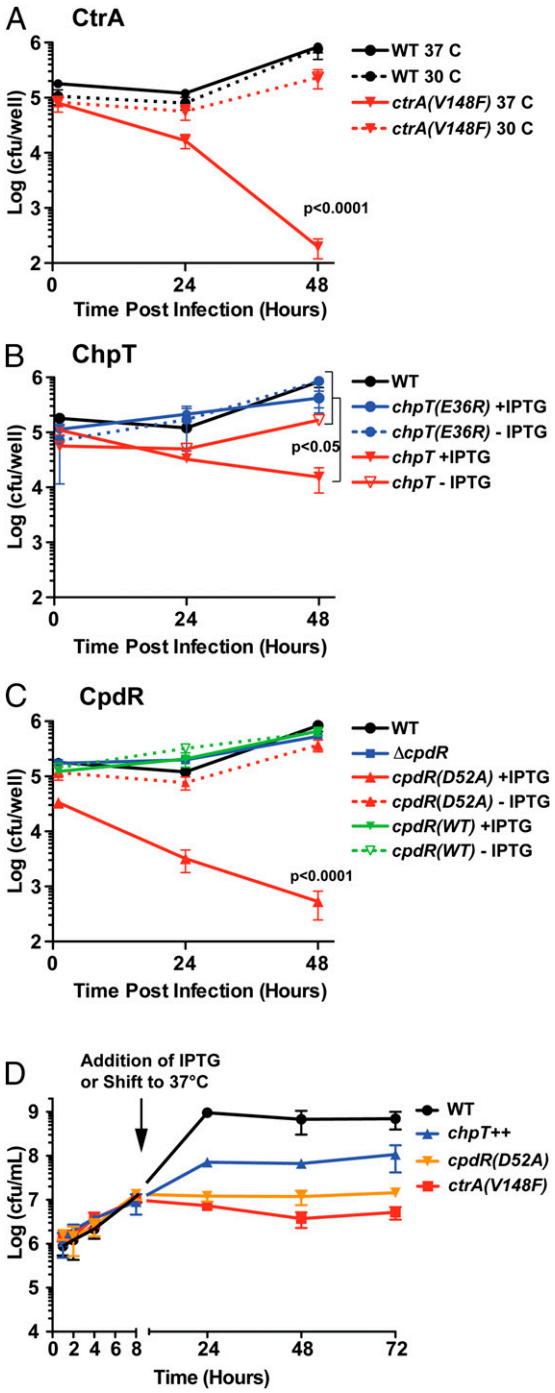

Fig. 4. The CckA–ChpT–CtrA–CpdR phosphorelay regulates intracellular replication, and survival of WT and mutant *B. abortus* strains in terminally differentiated THP-1 macrophages. (*A*) Enumeration (cfu per well) of the intracellular *ctrA(V148F)* temperature-sensitive strain recovered from THP-1 cells cultured at the nonpermissive (37 °C) and permissive (30 °C) temperatures. (*B*) Enumeration of intracellular *B. abortus* overexpressing *chpT* or (*C*) *cpdR* recovered from THP-1. (*D*) Growth and survival of WT and mutant *B. abortus* strains cultured axenically over 48 h in complex medium. Cultures were first grown for 8 h under conditions in which mutant alleles were not activated/induced [30 °C for *ctrA(V148F)* and without IPTG for *cpdR(WT)*$^{++}$ *and cpdR(D52A)*$^{++}$ strains]. Cultures were then shifted to inducing conditions [37 °C for *ctrA(V148F)* and adding IPTG to *cpdR(WT)*$^{++}$ and *cpdR(D52A)*$^{++}$]. Numbers indicate *B. abortus* viable cfu per milliliter of medium, recovered at time points through this culture procedure. Data points represent mean cfu of three independent samples ± SEM.

dimerization and histidine phosphotransfer (DHp) domain and a C-terminal domain that is structurally similar to the catalytic and ATP-binding (CA) domain found in HKs. A least-squares fit of the two monomers to each other shows that they are highly similar (rmsd = 0.33 Å on Cα). Within the structure, the DHp domains from each monomer dimerize to form a four-helix bundle (Fig. 5*A*). Small angle X-ray scattering (SAXS) data collected on ChpT in solution revealed a particle with radius of gyration (R_g) of 26.4 ± 0.4 Å at 15 μM concentration (Fig. S4*A*); this is consistent with R_g calculated (38) from the ChpT crystal structure (24.0 Å), providing evidence that ChpT is also a dimer in solution.

Although ChpT has strong similarity to classic HKs at the level of tertiary and quaternary structure, the pseudo-CA domain lacks regions required for ATP binding including the D-box, F-Box, and G-Box; ChpT also has a truncated ATP lid (Fig. S1*C*). ChpT retains the conserved N-box, which is known to bind a divalent cation (39), but we do not observe electron density consistent with ions or solvent in this region of the structure. Isothermal titration calorimetry (ITC) experiments demonstrate that ChpT, unlike multiple classes of HKs (40, 41), is unable to bind ATP (Fig. S4*B*). Based on these data, we conclude that *B. abortus* ChpT is unable to catalyze ATP hydrolysis and functions solely as a phosphotransferase (Fig. 2).

Structural Asymmetry in the ChpT–CtrA Signaling Complex. We have demonstrated that *B. abortus* ChpT is the central phosphotransferase in a pathway that begins with CckA∼P and terminates at the receiver domains of CtrA and CpdR (Fig. 2). To further define the molecular basis of signaling through the CckA–ChpT–CtrA–CpdR system, we solved the structure of ChpT bound to the receiver domain of CtrA ($CtrA_{REC}$) (PDB ID code 4QPJ). Both ChpT and $CtrA_{REC}$ were purified separately and combined at an equimolar ratio before screening for crystals. The complex formed crystals of space group $P3_221$ (cell dimensions a = 124.95, b = c = 136.33 Å) that diffracted to 2.7-Å resolution. We solved the structure of the ChpT–$CtrA_{REC}$ complex by molecular replacement using the ChpT structure as a search model; the solution provided sufficient phase information to build models for the bound $CtrA_{REC}$ domains. The structure was refined to R_{work} = 0.175 and R_{free} = 0.222; all crystallographic data are summarized in Table S2.

The structure reveals two unphosphorylated $CtrA_{REC}$ monomers positioned against opposing DHp domains of the ChpT dimer, forming a 2:2 complex ($ChpT_2$–$CtrA_2$) (Fig. 5*B*). We hereafter annotate the two phosphotransferase monomers as ChpT(A) and ChpT(B); the two REC domains are annotated CtrA(C) and CtrA(D). The overall structure of ChpT in complex with $CtrA_{REC}$ is largely unchanged relative to the isolated structure of ChpT (rmsd of 0.62 Å on Cα). This stands in contrast to *Thermotoga maritima* HK853, which undergoes a large conformational change about the DHp-CA domain linker upon binding to its receiver substrate RR468 (42). Unlike HK853 bound to RR468, or Spo0B phosphotransferase bound to Spo0F (43), the complex is not fully symmetrical. Notably, the side-chain orientation of the ChpT phosphorylation sites (H22) show marked asymmetry between ChpT(A) and ChpT(B). In ChpT(A), the εN atom of H22 is positioned 5.9 Å away and is aligned with the δO atom of CtrA(C) phosphoacceptor residue D51 (Fig. 5*C*). This measured distance is consistent with defined His–Asp (εN–δO) distances in the Spo0B–Spo0F (43) and the YPD1–SLN1 (44) phosphotransfer complexes and is ∼2 Å shorter than the corresponding εN–δO distances in the unmodified HK853–RR468 complex (42). In terms of His–Asp distance, ChpT(A) thus seems poised for facile phosphotransfer to CtrA(C) without the need for significant conformational change in either ChpT or CtrA. On the opposing side of the ChpT dimer, the side chains of ChpT(B) H22 and CtrA(D) D51 are in different conformations (Fig. 5*C*): The εN atom of H22 is positioned >12 Å away and is not aligned with the D51 δO atom of CtrA(D). This half of the ChpT–CtrA complex is therefore not competent to

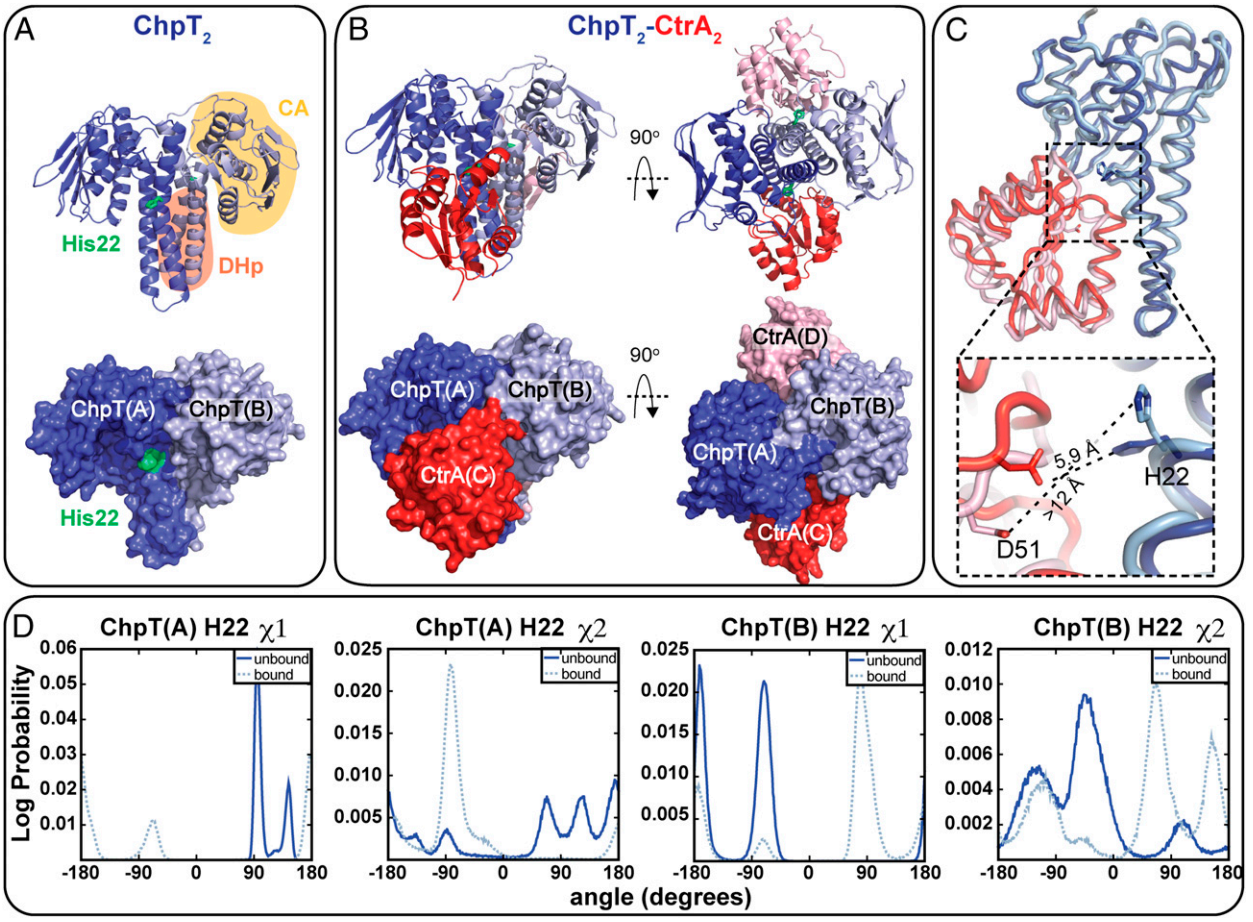

Fig. 5. Molecular structures of *B. abortus* ChpT and ChpT– $CtrA_{REC}$ complex. (*A*) Ribbon (*Top*) and surface views (*Bottom*) of homodimeric *B. abortus* ChpT at 1.7-Å resolution (PDB ID code 4QPK). One ChpT monomer is drawn in dark blue and one in light blue. The conserved site of ChpT phosphorylation, His22, is highlighted green; DHp (highlighted pink) and CA-like domains (highlighted yellow) of ChpT are labeled. (*B*) Ribbon (*Top*) and surface views (*Bottom*) of the 2:2 ChpT-$CtrA_{REC}$ complex at 2.7-Å resolution (PDB ID code 4QPJ); diagram illustrates two CtrA receiver domain (REC) monomers (in red and pink) bound to a central homodimer of ChpT (ChpT monomers in dark blue and light blue). (*C*) Least-squares Cα fit of the two halves of ChpT–$CtrA_{REC}$ complex: ChpT(A) dark blue, ChpT(B) light blue, $CtrA_{REC}$(C) dark red, and $CtrA_{REC}$(D) pink. Distances between ChpT(A)–CtrA(C) and ChpT(B)–CtrA(D) phosphoryltransfer residues (ChpT H22 and CtrA D51) are labeled in the expanded box. (*D*) Log probability of ChpT(A) and ChpT(B) H22 χ1 and χ2 rotamer angle occupancy in the ChpT (unbound; solid blue) and in the $ChpT_2$–$CtrA_2$ complex structures (bound; light dotted blue) based on MD simulations (*Materials and Methods*); distributions represent Gaussian fluctuations of H22 conformation about a local equilibrium state.

catalyze His–Asp phosphotransfer without a significant change in protein conformation. Overall, the absence of large-scale conformational change in ChpT upon receiver binding provides evidence that the structural mechanism of phosphotransfer from ChpT to its substrates is distinct from HK-receiver phosphotransfer defined in the *T. maritima* HK853–RR468 system, because large structural changes are observed in HK853 upon RR468 binding. ChpT H22 and CtrA D51 asymmetry, as it may relate to phosphotransfer, is discussed in a later section of this manuscript.

An analysis of the CtrA structure across each half of the ChpT dimer reveals additional asymmetric features of the signaling complex. Both CtrA molecules retain the standard αβα sandwich fold observed in other REC domain structures (23). However, an alignment of CtrA(C) to CtrA(D) revealed a higher Cα rmsd (1.6 Å) than observed in ChpT(A)–ChpT(B) alignments. Approximately half the intermolecular interactions within the ChpT–CtrA complex occur through the α1 helix of ChpT and the β1–α1, β3–α3, and β5–α5 loops of CtrA; these contacts are consistent with known HK–REC interfaces (45). Five ChpT residues that interact with CtrA (N33, E36, E40, K96, and H177) are observed on each half of the dimer, but there are significant differences in how CtrA(C) and CtrA(D) contact ChpT. In particular, a set of hydrogen bonds between E34 of CtrA(D) helix α2 and residues R129, R153, and H177 of ChpT(B) are unique to that interface (Fig. 5*C*). There is clear asymmetry in the ChpT–CtrA contact surface on either side of the complex: Contact between ChpT(A) and CtrA(C) is more extensive than ChpT(B) and CtrA(D) (935 $Å^2$ versus 829 $Å^2$ buried surface area). These structural data predict that the phosphotransfer "competent" half of the complex [i.e., ChpT(A) to CtrA(C)] may form a higher-affinity interface than ChpT(B) to CtrA(D). Indeed, calculations based on total solvation energies of isolated and interfacing structure (46) suggest an approximate 4.5 kcal/mol difference in free energy between the two ChpT–CtrA interfaces.

Conformational Asymmetry and Dynamics of the ChpT Phosphorylation Site. The crystal structure of ChpT bound to CtrA raised the question of whether conformational and dynamical asymmetry of the ChpT phosphorylation site (H22) was a genuine feature of this signaling complex. To begin to address this question, we performed molecular dynamics (MD) simulations on our experimental structures of the ChpT dimer (1,800 ns) and the $ChpT_2$–$CtrA_2$ heterotetramer (900 ns) in a fully atomistic system with explicit solvent. These simulations were aimed at testing whether the dynamics of

ChpT H22 in the isolated ChpT structure and in the ChpT–CtrA complex are inherently asymmetric across the twofold ChpT dimer axis.

As described above, our crystal structure of ChpT–CtrA revealed two distinct conformations of the ChpT H22. MD simulations show that H22 stably occupies multiple χ_1/χ_2 rotamer angles on chains A and B, both when bound and unbound to CtrA (Fig. 5*D*). When not bound to CtrA, ChpT(A) H22 evinces substantial heterogeneity: Five stable rotameric states are apparent. The rotamer conformations occupied by H22 differ in each ChpT monomer both when bound and not bound to CtrA. These results provide evidence that the significant asymmetry we observe in conformations of ChpT H22 in our complex crystal structure is not an artifact of crystallization, but rather reflects true asymmetry in protein conformational dynamics at this site. We conclude that small differences in side-chain and backbone structure, likely enforced by ChpT–ChpT and ChpT–CtrA interaction at the quaternary level, affect the energy landscape of H22 conformational transitions. This in turn affects the primary rotamer conformations that H22 samples on each side of the ChpT dimer.

Structural and Functional Analysis of ChpT Phosphoryltransfer. The experimental crystal structures of *B. abortus* ChpT and the 2:2 ChpT–$CtrA_{REC}$ complex provide a foundation for understanding the molecular basis of phosphoryltransfer through the CckA–ChpT–CtrA–CpdR system. Using these data, we constructed point mutations in components of the pathway to test predictions of our structural models in vitro. We initially tested whether ChpT residues observed to interact with CtrA in our crystal structure are required for the initial phosphotransfer step in this pathway (i.e., CckA to ChpT). In our experimental structure, three residues within the DHp domain of ChpT (N33, E36, and E40) and three residues within the CA domain (K96, R153, and H177) interact extensively with CtrA in the asymmetric $ChpT_2$–$CtrA_2$ complex (Fig. 5*B*). We generated and purified ChpT proteins with combinations of alanine mutations in the CtrA-interacting residues of the DHp and CA domains. We then assayed these mutant proteins for their ability to receive phosphoryl groups from equimolar CckA~P over the course of a 5-min reaction. Neither the ChpT(N33A,E36A,E40A) nor ChpT(K96A,R156A,H177A) triple point mutant proteins exhibited a measurable defect in phosphotransfer with CckA (Fig. 6*A*). Although these residues make direct CtrA contact in the crystal structure, our results suggest that this interface is robust to truncation of larger side chains; loss of contact residues permitted near WT levels of phosphotransfer. Alternatively, different residues in ChpT could be required for interaction with CckA–REC and CtrA. We further generated ChpT(N33R), ChpT(E36R), and ChpT(E40R) mutant proteins. Addition of these single, larger, charged residues to the interaction interface reduced phosphotransfer ~4–10 fold (Fig. 6*A*). Defects in phosphotransfer were not a result of a large-scale unfolding or disruption of ChpT structure as assayed by CD spectroscopy of purified ChpT mutant proteins (Fig. S4*C*).

We further investigated whether mutations in this region of ChpT are important for phosphotransfer to CtrA and CpdR. Not surprisingly, both the ChpT(N33A,E36A,E40A) and ChpT(K96A, R156A,H177A) mutant proteins exhibited only modest defects in phosphotransfer to both CtrA and CpdR (Fig. 6 *B* and *C*). However, ChpT(N33R), ChpT(E36R), and ChpT(E40R) mutants displayed severe defects in phosphotransfer to CtrA and CpdR; the ChpT(E36R) mutant protein displayed the greatest defect in phosphotransfer as indicated by ~95% reduction of CtrA~P and CpdR~P levels relative to ChpT(WT). Finally, we sought to test the role of an important residue of CtrA/CpdR helix α1 in phosphotransfer with ChpT. Helix α1 residue S15 of CtrA interacts directly with ChpT(A) in our crystal structure (Fig. 5) and is important for HK–receiver interactions in a number of different systems (42, 47, 48). We substituted CtrA(S15) and the homologous position in CpdR(F16) to arginine and assayed CckA–ChpT-dependent phosphorylation. These mutations resulted in an approximate 50% reduction in the level of CpdR~P and a ~90% reduction in CtrA~P (Fig. 6 *B* and *C*).

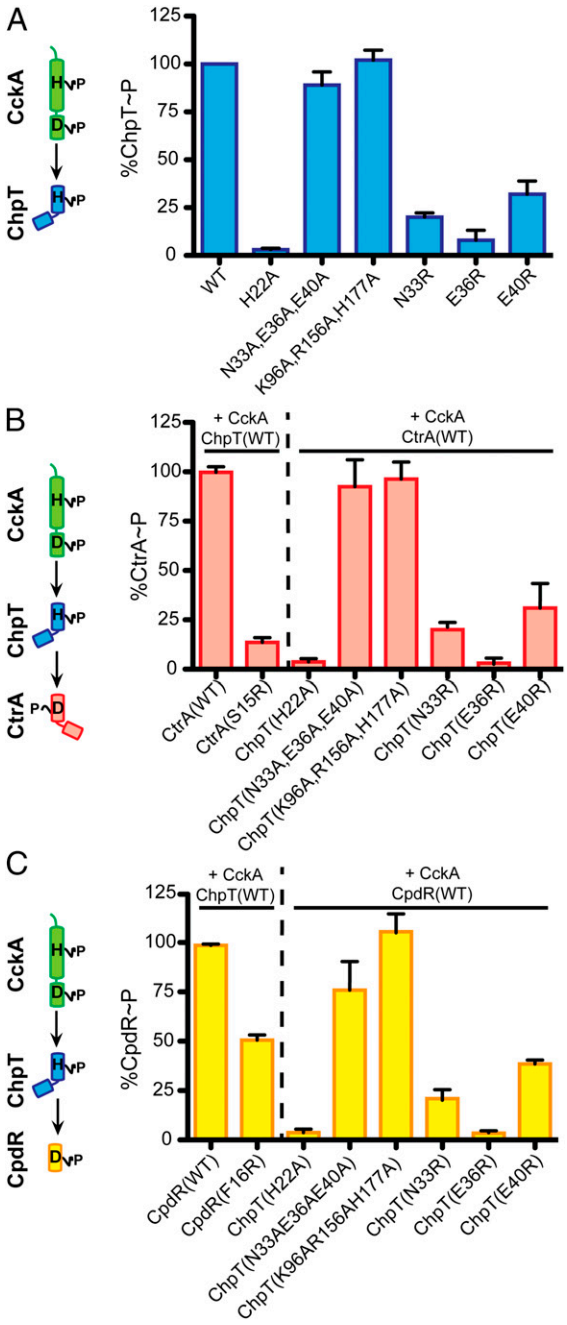

Fig. 6. A structural analysis of phosphoryltransfer. (*A*) Phosphoryltransfer from phospho-CckA (CckA~P) to an equimolar concentration of WT and mutant ChpT (ChpT point mutations labeled on axis). (*B*) Phosphoryltransfer from CckA~P to CtrA(WT) and CtrA(S15R) proteins in the presence of WT or mutant ChpT proteins. (*C*) Phosphoryltransfer from CckA~P to CpdR(WT) and CpdR(F16R) proteins in the presence of WT or mutant ChpT proteins. All phosphotransfer reactions are normalized to phosphotransfer reactions performed with WT controls (100%); mean ± SEM is shown for three independent replicates.

To further assay the functional significance of a molecular interaction defined in our crystal structures, we expressed the *chpT(E36R)* mutant allele in *B. abortus* cells (Fig. 3). Although

overexpression of WT *chpT* (*chpT*$^{++}$) results in a defect in cell morphology, DNA content, and intracellular survival, overexpression of *chpT(E36R)* does not have a statistically significant effect on any of these phenotypes (Figs. 3 and 4). This result is consistent with the inability of *chpT(E36R)* to facilitate phosphoryltransfer in vitro (Fig. 6). As a control, we confirmed that WT ChpT and the ChpT(E36R) alleles were expressed at similar levels in the *B. abortus* cell (Fig. S2*D*).

Discussion

Protein phosphorelays regulate many important processes in bacteria, including asymmetric cell division, sporulation, and multicellular development (49, 50). The conserved CckA–ChpT–CtrA–CpdR phosphorelay controls transcription of a diverse set of genes involved in multiple aspects of α-proteobacterial cellular biology (8, 10, 14). To date, the identities and functions of the genes encoding this pathway in the intracellular pathogen *B. abortus* had remained largely undefined. We have identified and biochemically reconstituted the complete *B. abortus* CckA–ChpT–CtrA–CpdR system in vitro and provide evidence that it comprises an essential and specific phosphorelay that regulates replication, cell division, and survival in the intracellular niche. ChpT is central in this pathway and shuttles phosphoryl groups between the HK CckA and two receiver substrates, CtrA and CpdR. CtrA is a classical DNA-binding response regulator, whereas CpdR is a single domain receiver that regulates steady-state CtrA levels in the cell (Fig. 3). Our data support a model in which the regulatory topology of this pathway is conserved between *B. abortus* and *C. crescentus*, two α-proteobacterial species that inhabit widely different environmental niches and have distinct cellular features.

We have discovered that *B. abortus* mutants defective in signaling through this pathway have no deficiency in entry into a human macrophage cell line but exhibit reduced intracellular survival over a 48-h timescale (Fig. 4). This survival defect is specific to the intracellular niche because expression of conditional *ctrA(V148F)*, *chpT*$^{++}$, and *cpdR(D52A)*$^{++}$ alleles that strongly perturb the phosphorelay does not result in cell death in axenic culture (Fig. 4*D*). This result raises the question of what specific genes are under transcriptional control of the CckA–ChpT–CtrA–CpdR system, and which of these genes are required for survival of *B. abortus* inside mammalian cells. A previous study has identified a CtrA binding site in front of the cell division protein *ftsE* (15), which is consistent with observed cell division defects. However, there are certainly other direct targets of this essential response regulator, many of which are likely to be important for the intracellular lifestyle of *B. abortus*. Like the PhoPQ two-component system of *Salmonella*, this phosphorelay may control cell surface remodeling during infection, which is known to be important for intracellular survival (51).

The transcriptional output of conserved phosphorelays like the CckA–ChpT–CtrA–CpdR system (14) or more simple, archetypal two-component systems like FixL–FixJ (52) are often tailored to the unique physiologies of the species in which they are encoded. We note that consensus CtrA binding sites, based on published *B. abortus* CtrA targets (15), are present in front of several known *B. abortus* virulence factors including superoxide dismutase (*sodC*) and flagellar regulatory gene *ftcR* (53, 54). Defining genes in the *Brucella* CtrA regulon that uniquely control its function as a facultative intracellular pathogen is an important area of future investigation.

The structure of ChpT is related to classic HKs and is distinct from phosphotransferase proteins like Ypd1, which lack a CA-like domain (44). It is likely that ChpT arose through HK gene duplication and subsequently evolved to function solely as a phosphotransferase. Indeed, the ChpT CA domain does not bind ATP, supporting a model in which ChpT structure and function have diverged from an ancestral HK (32). This raises the question of what function ChpT–CA plays if it does not bind nucleotide. It is possible that the ChpT–CA domain is conserved because it has an important structural role in binding to receiver domain substrates. Certainly, the crystal structure of ChpT bound to $CtrA_{REC}$ reveals several direct interactions between $CtrA_{REC}$ and ChpT–CA (Fig. 5 and Fig. S5 *B*, *C*, and *D*) that are related to those in structurally defined HK–REC systems (42). The ChpT–CA domain may simply enhance stability of ChpT–REC complexes and facilitate efficient phosphotransfer. Alternatively, ChpT–CA may confer additional regulatory capacity on the system. For example, the binding of different nucleotide forms by the CA domain can modulate both kinase and phosphatase activities of HKs (18, 55, 56). Although ChpT does not bind ATP, there may be other small molecule ligands that can serve to regulate interaction of ChpT with its receiver substrates. The clear presence of a glycerol molecule in the electron density maps of the ChpT–CA binding pocket (Fig. S5*A*) demonstrates that CA has the capacity to accommodate small molecules and suggests that small-molecule binding to ChpT–CA could allow for the integration of additional signals into this important pathway.

The experimental structure of the ChpT–CtrA heterotetramer revealed three residues in the DHp-like domain (N33, E36, and E40) and three residues in the CA-like domain of ChpT (K96, R153, and H177) that interact with CtrA on each half of the ChpT homodimer (Fig. 5*B*). These ChpT residues correspond to the so-called specificity residues that govern specific HK-to-response regulator (RR) phosphoryltransfer (48, 57). Our structure thus provides evidence that the ChpT phosphotransferase interacts with its cognate substrates in a manner that is structurally similar to classic HK–RR interactions. Alanine mutagenesis showed that the ChpT–RR structural interface is robust to multiple substitutions under the tested in vitro conditions. This result is consistent with mutagenesis studies of the kinases CrdS from *Myxococcus xanthus* and EnvZ from *Escherichia coli*, in which substitution of select CrdS and EnvZ specificity residues had minimal impact on phosphoryltransfer to their cognate RRs in vitro (58, 59). However, it may be the case that these substitutions affect phosphoryltransfer specificity in vitro or signaling in *B. abortus* cells.

A notable structural feature reported in this study is asymmetry in the positions of the ChpT phosphorylation site (H22) and the CtrA phosphoryl receiver residue (D51) (Fig. 5 *C* and *D*). H22 occupies identical rotamer conformations in the structure of ChpT alone but two distinct rotamer conformations on each side of the ChpT homodimer in the 2:2 ChpT–CtrA complex. On one side of the complex, H22 is in line with D51 of CtrA, which is well-positioned to receive a phosphoryl group. On the opposite side of the complex, both H22 and D51 adopt different rotamer conformations and would not be able to undergo phosphotransfer without a large change in H22 and D51 side-chain conformation. The half of the complex that is positioned to undergo phosphotransfer has a larger ChpT–CtrA contact surface than the half that is incompatible with phosphotransfer. These structural data suggest that the ChpT dimer has at least two distinct interaction modes with CtrA substrate: one that is competent to catalyze phosphotransfer and one that buries less ChpT–REC surface area and is structurally incompetent for phosphotransfer. Although the asymmetry of ChpT–CtrA interaction observed in our structure may be a function of embedment in the crystal lattice, long-time-scale MD simulations presented herein support a model in which the histidine phosphorylation sites on each half of the ChpT dimer have distinct structural and dynamical properties, particularly in the context of the 2:2 ChpT–CtrA complex (Fig. 5 *B–D* and Fig. S5). Thus, at any instant only one side of the ChpT–CtrA complex may be competent to undergo a His–Asp phosphotransfer reaction. Our structures and simulations do not directly address the effects of adding phosphoryl groups to H22 or D51. The affects of

phosphoryl addition to H22 or D51 on protein structure and dynamics are a topic of ongoing investigation.

We note that structural asymmetry has been reported for other HKs. Thus, the structural and dynamical asymmetry we observe across the central twofold axis of the 2:2 ChpT–CtrA heterodimer may reflect a general (but not necessarily universal) feature of two-component phosphorelays. Indeed, it is established that the autophosphorylation equilibria of each subunit of dimeric *E. coli* NtrB differ by nearly two orders of magnitude (60). The structures of HKs HK853 (34), DesK (61), YF1 (62), VicK (36), and CpxA (35) adopt different tertiary structures in the frame of the central HK dimer axis. Structures of VicK, YF1, and CpxA in particular show highly asymmetric positioning of the CA domain: One CA is proximal to the site of histidine phosphorylation and the second CA domain is distal. Moreover, recent work on *T. maritima* HK853 provides structural evidence for asymmetry in the histidine autokinase reaction (63), even though the ATP-binding CA domains occupy symmetrical positions in the unphosphorylated structure (34). Although ChpT is not a bona fide HK, our study provides evidence that this protein has retained some structural features common to other two-component His–Asp phosphorelay systems and may thus serve as an excellent model to investigate the structural and dynamical mechanisms that underpin function of these complex regulatory systems.

Materials and Methods

Bacterial Culture and Strain Construction. All strains and primers used in this study are detailed in Tables S3 and S4. *E. coli* strains were constructed using routine cloning techniques. All *B. abortus* strains were maintained and constructed using previously described techniques (64) under biosafety level 3 (BSL3) conditions per Centers for Disease Control and Prevention (CDC) rules and regulations governing the use of select agents. Further details on strain generation and maintenance are provided in *Supporting Information*.

In Vitro Kinase and Phosphotransfer Assays. Genes encoding proteins to be overexpressed were cloned into pET28a (Novagen), expressed in Rosetta *E. coli* (DE3), and purified using an N-terminal His_6-tag. All kinase and phosphotransfer reactions were performed following previously published methods (20, 21, 65). For complete protocols see *Supporting Information*.

Crystallization of ChpT and the ChpT–CtrA Complex. All crystallization conditions used the hanging drop vapor diffusion technique. The structure of ChpT alone was obtained by mixing $CckA_{soluble}$ (20 mg·mL^{-1} final) and ChpT (4.7 mg·mL $^{-1}$ final) and seeding using a horse hair in the following crystallization buffer: 0.2 M ammonium sulfate, 0.1 M sodium acetate pH 5.5, and 10% (wt/vol) PEG 2000 MME. The $ChpT_2$–$CtrA_2$ complex was obtained by mixing ChpT (8.4 mg·mL $^{-1}$) and CtrA (5.3 mg·mL $^{-1}$) after concentration using the following crystallization buffer: 0.1 M Hepes pH 7.0 and 8% (wt/vol) PEG 8000. After mixing 1.5 μL of protein solution and 1.5 μL of crystallization buffer against 500 μL of crystallization buffer in the well, all crystals grew for 7 d and were mounted after soaking for 1 min in crystallization buffer supplemented with 25% (vol/vol) glycerol.

Crystallographic Data Collection, Processing, Phasing, and Refinement. All diffraction data were collected on beamline 21-ID-F (Life Sciences Collaborative Access Team, Advanced Photon Source) and reduced using the HKL 2000 software suite. All structures were solved by molecular replacement in PHENIX (66) using models that were initially based off *C. crescentus* ChpT (33). Model building and refinement was conducted using Coot and PHENIX, accessed through the SBGrid consortium (67). Coordinates of the *B. abortus* ChpT (PDB ID code 4QPK) and the 2:2 ChpT–CtrA complex (PDB ID code 4QPJ) have been deposited in the Protein Data Bank.

Biophysical Analyses of ChpT Structure. Analyses of ChpT by CD spectroscopy, ITC, and SAXS were performed using previously published methods (59, 68, 69) and are described in detail in *Supporting Information*. SAXS data on ChpT were collected at the Advanced Photon Source beamline 18-ID (BioCAT).

Molecular Dynamics Simulations. Fully atomistic models of ChpT, CtrA, and the ChpT–CtrA complex were constructed based on the crystallographic data presented in this study. The simulations were run for 1,851, 1,000, and 886 ns, respectively. Further details are provided in *Supporting Information*.

Imaging and Analysis of *Brucella* Cells. Before analysis by LM, flow cytometry, and CryoEM, *B. abortus* cells were fixed following established BSL3 *B. abortus* protocols at the University of Chicago Ricketts Laboratory. All infection assays using differentiated THP-1 macrophages used an MOI of 100. All results presented are the mean ± SEM. Details of sample preparation and analysis are outlined in *Supporting Information*.

ACKNOWLEDGMENTS. We thank Aretha Fiebig and members of the S.C. laboratory for discussions and guidance during the preparation of this manuscript and Elena Solomaha and Ryan Duggan for technical assistance. This project has been funded in whole or in part with federal funds from NIH–National Institute of Allergy and Infectious Diseases Grants U19 AI107792 and R01 AI107159 (to S.C.). J.W.W. is supported by NIH Ruth Kirschstein Postdoctoral Fellowship F32 GM109661. Funding for LS-CAT Sector 21 was provided by the Michigan Economic Development Corporation and the Michigan Technology Tri-Corridor Grant 085P1000817. Small angle X-ray scattering at Advanced Photon Source–BioCAT is supported by NIH Grant P41 GM103622.

1. Pappas G, Papadimitriou P, Akritidis N, Christou L, Tsianos EV (2006) The new global map of human brucellosis. *Lancet Infect Dis* 6(2):91–99.
2. Atluri VL, Xavier MN, de Jong MF, den Hartigh AB, Tsolis RM (2011) Interactions of the human pathogenic Brucella species with their hosts. *Annu Rev Microbiol* 65:523–541.
3. Dean AS, et al. (2012) Clinical manifestations of human brucellosis: A systematic review and meta-analysis. *PLoS Negl Trop Dis* 6:e1929.
4. Batut J, Andersson SG, O'Callaghan D (2004) The evolution of chronic infection strategies in the alpha-proteobacteria. *Nat Rev Microbiol* 2(12):933–945.
5. Philippot L, et al. (2010) The ecological coherence of high bacterial taxonomic ranks. *Nat Rev Microbiol* 8(7):523–529.
6. McAdams HH, Shapiro L (2009) System-level design of bacterial cell cycle control. *FEBS Lett* 583(24):3984–3991.
7. Tsokos CG, Laub MT (2012) Polarity and cell fate asymmetry in Caulobacter crescentus. *Curr Opin Microbiol* 15(6):744–750.
8. Biondi EG, et al. (2006) Regulation of the bacterial cell cycle by an integrated genetic circuit. *Nature* 444(7121):899–904.
9. Iniesta AA, McGrath PT, Reisenauer A, McAdams HH, Shapiro L (2006) A phosphosignaling pathway controls the localization and activity of a protease complex critical for bacterial cell cycle progression. *Proc Natl Acad Sci USA* 103(29):10935–10940.
10. Laub MT, Chen SL, Shapiro L, McAdams HH (2002) Genes directly controlled by CtrA, a master regulator of the Caulobacter cell cycle. *Proc Natl Acad Sci USA* 99(7): 4632–4637.
11. Leung MM, Brimacombe CA, Beatty JT (2013) Transcriptional regulation of the Rhodobacter capsulatus response regulator CtrA. *Microbiology* 159(Pt 1):96–106.
12. Wang H, et al. (2014) The CtrA phosphorelay integrates differentiation and communication in the marine alphaproteobacterium Dinoroseobacter shibae. *BMC Genomics* 15:130.
13. Zan J, Heindl JE, Liu Y, Fuqua C, Hill RT (2013) The CckA-ChpT-CtrA phosphorelay system is regulated by quorum sensing and controls flagellar motility in the marine sponge symbiont Ruegeria sp. KLH11. *PLoS ONE* 8(6):e66346.
14. De Nisco NJ, Abo RP, Wu CM, Penterman J, Walker GC (2014) Global analysis of cell cycle gene expression of the legume symbiont Sinorhizobium meliloti. *Proc Natl Acad Sci USA* 111(9):3217–3224.
15. Bellefontaine AF, et al. (2002) Plasticity of a transcriptional regulation network among alpha-proteobacteria is supported by the identification of CtrA targets in Brucella abortus. *Mol Microbiol* 43(4):945–960.
16. Robertson GT, et al. (2000) The Brucella abortus CcrM DNA methyltransferase is essential for viability, and its overexpression attenuates intracellular replication in murine macrophages. *J Bacteriol* 182(12):3482–3489.
17. Ulrich LE, Zhulin IB (2010) The MiST2 database: A comprehensive genomics resource on microbial signal transduction. *Nucleic Acids Res* 38(Database issue):D401–D407.
18. Gutu AD, Wayne KJ, Sham LT, Winkler ME (2010) Kinetic characterization of the WalRKSpn (VicRK) two-component system of Streptococcus pneumoniae: Dependence of WalKSpn (VicK) phosphatase activity on its PAS domain. *J Bacteriol* 192(9):2346–2358.
19. Willett JW, Kirby JR (2011) CrdS and CrdA comprise a two-component system that is cooperatively regulated by the Che3 chemosensory system in Myxococcus xanthus. *MBio* 2(4):e00110–e00111.
20. Willett JW, et al. (2013) Specificity residues determine binding affinity for two-component signal transduction systems. *MBio* 4(6):e00420–e13.
21. Skerker JM, Prasol MS, Perchuk BS, Biondi EG, Laub MT (2005) Two-component signal transduction pathways regulating growth and cell cycle progression in a bacterium: A system-level analysis. *PLoS Biol* 3(10):e334.
22. Laub MT, Biondi EG, Skerker JM (2007) Phosphotransfer profiling: Systematic mapping of two-component signal transduction pathways and phosphorelays. *Methods Enzymol* 423:531–548.
23. Stock AM, Robinson VL, Goudreau PN (2000) Two-component signal transduction. *Annu Rev Biochem* 69:183–215.

24. Barnett MJ, Hung DY, Reisenauer A, Shapiro L, Long SR (2001) A homolog of the CtrA cell cycle regulator is present and essential in Sinorhizobium meliloti. *J Bacteriol* 183(10):3204–3210.
25. Brilli M, et al. (2010) The diversity and evolution of cell cycle regulation in alpha-proteobacteria: A comparative genomic analysis. *BMC Syst Biol* 4:52.
26. Kim J, Heindl JE, Fuqua C (2013) Coordination of division and development influences complex multicellular behavior in Agrobacterium tumefaciens. *PLoS ONE* 8(2):e56682.
27. Quon KC, Marczynski GT, Shapiro L (1996) Cell cycle control by an essential bacterial two-component signal transduction protein. *Cell* 84(1):83–93.
28. Jacobs C, Domian IJ, Maddock JR, Shapiro L (1999) Cell cycle-dependent polar localization of an essential bacterial histidine kinase that controls DNA replication and cell division. *Cell* 97(1):111–120.
29. Smith SC, et al. (2014) Cell cycle-dependent adaptor complex for ClpXP-mediated proteolysis directly integrates phosphorylation and second messenger signals. *Proc Natl Acad Sci USA* 111(39):14229–14234.
30. Brown PJB, et al. (2012) Polar growth in the Alphaproteobacterial order Rhizobiales. *Proc Natl Acad Sci USA* 109(5):1697–1701.
31. Pincus Z, Theriot JA (2007) Comparison of quantitative methods for cell-shape analysis. *J Microsc* 227(Pt 2):140–156.
32. Blair JA, et al. (2013) Branched signal wiring of an essential bacterial cell-cycle phosphotransfer protein. *Structure* 21(9):1590–1601.
33. Fioravanti A, et al. (2012) Structural insights into ChpT, an essential dimeric histidine phosphotransferase regulating the cell cycle in Caulobacter crescentus. *Acta Crystallogr Sect F Struct Biol Cryst Commun* 68(Pt 9):1025–1029.
34. Marina A, Waldburger CD, Hendrickson WA (2005) Structure of the entire cytoplasmic portion of a sensor histidine-kinase protein. *EMBO J* 24(24):4247–4259.
35. Mechaly AE, Sassoon N, Betton JM, Alzari PM (2014) Segmental helical motions and dynamical asymmetry modulate histidine kinase autophosphorylation. *PLoS Biol* 12(1):e1001776.
36. Wang C, et al. (2013) Mechanistic insights revealed by the crystal structure of a histidine kinase with signal transducer and sensor domains. *PLoS Biol* 11(2):e1001493.
37. Varughese KI, Madhusudan, Zhou XZ, Whiteley JM, Hoch JA (1998) Formation of a novel four-helix bundle and molecular recognition sites by dimerization of a response regulator phosphotransferase. *Mol Cell* 2(4):485–493.
38. Svergun D, Barberato C, Koch MHJ (1995) CRYSOL - A program to evaluate x-ray solution scattering of biological macromolecules from atomic coordinates. *J Appl Cryst* 28:768–773.
39. Dutta R, Yoshida T, Inouye M (2000) The critical role of the conserved Thr247 residue in the functioning of the osmosensor EnvZ, a histidine Kinase/Phosphatase, in Escherichia coli. *J Biol Chem* 275(49):38645–38653.
40. Alexandre MT, et al. (2010) Electronic and protein structural dynamics of a photosensory histidine kinase. *Biochemistry* 49(23):4752–4759.
41. Bilwes AM, Quezada CM, Croal LR, Crane BR, Simon MI (2001) Nucleotide binding by the histidine kinase CheA. *Nat Struct Biol* 8(4):353–360.
42. Casino P, Rubio V, Marina A (2009) Structural insight into partner specificity and phosphoryl transfer in two-component signal transduction. *Cell* 139(2):325–336.
43. Varughese KI, Tsigelny I, Zhao H (2006) The crystal structure of beryllofluoride Spo0F in complex with the phosphotransferase Spo0B represents a phosphotransfer pretransition state. *J Bacteriol* 188(13):4970–4977.
44. Xu Q, Porter SW, West AH (2003) The yeast YPD1/SLN1 complex: Insights into molecular recognition in two-component signaling systems. *Structure* 11(12):1569–1581.
45. Capra EJ, Laub MT (2012) Evolution of two-component signal transduction systems. *Annu Rev Microbiol* 66:325–347.
46. Krissinel E, Henrick K (2007) Inference of macromolecular assemblies from crystalline state. *J Mol Biol* 372(3):774–797.
47. Laub MT, Goulian M (2007) Specificity in two-component signal transduction pathways. *Annu Rev Genet* 41:121–145.
48. Skerker JM, et al. (2008) Rewiring the specificity of two-component signal transduction systems. *Cell* 133(6):1043–1054.
49. Kroos L (2007) The Bacillus and Myxococcus developmental networks and their transcriptional regulators. *Annu Rev Genet* 41:13–39.
50. Shapiro L, McAdams HH, Losick R (2009) Why and how bacteria localize proteins. *Science* 326(5957):1225–1228.
51. Guo L, et al. (1997) Regulation of lipid A modifications by Salmonella typhimurium virulence genes phoP-phoQ. *Science* 276(5310):250–253.
52. Crosson S, McGrath PT, Stephens C, McAdams HH, Shapiro L (2005) Conserved modular design of an oxygen sensory/signaling network with species-specific output. *Proc Natl Acad Sci USA* 102(22):8018–8023.
53. Gee JM, et al. (2005) The Brucella abortus Cu,Zn superoxide dismutase is required for optimal resistance to oxidative killing by murine macrophages and wild-type virulence in experimentally infected mice. *Infect Immun* 73(5):2873–2880.
54. Léonard S, et al. (2007) FtcR is a new master regulator of the flagellar system of Brucella melitensis 16M with homologs in Rhizobiaceae. *J Bacteriol* 189(1):131–141.
55. Igo MM, Ninfa AJ, Stock JB, Silhavy TJ (1989) Phosphorylation and dephosphorylation of a bacterial transcriptional activator by a transmembrane receptor. *Genes Dev* 3(11): 1725–1734.
56. Jiang P, Atkinson MR, Srisawat C, Sun Q, Ninfa AJ (2000) Functional dissection of the dimerization and enzymatic activities of Escherichia coli nitrogen regulator II and their regulation by the PII protein. *Biochemistry* 39(44):13433–13449.
57. Podgornaia AI, Laub MT (2013) Determinants of specificity in two-component signal transduction. *Curr Opin Microbiol* 16(2):156–162.
58. Capra EJ, et al. (2010) Systematic dissection and trajectory-scanning mutagenesis of the molecular interface that ensures specificity of two-component signaling pathways. *PLoS Genet* 6(11):e1001220.
59. Willett JW, Kirby JR (2012) Genetic and biochemical dissection of a HisKA domain identifies residues required exclusively for kinase and phosphatase activities. *PLoS Genet* 8(11):e1003084.
60. Jiang P, Peliska JA, Ninfa AJ (2000) Asymmetry in the autophosphorylation of the two-component regulatory system transmitter protein nitrogen regulator II of Escherichia coli. *Biochemistry* 39(17):5057–5065.
61. Albanesi D, et al. (2009) Structural plasticity and catalysis regulation of a thermosensor histidine kinase. *Proc Natl Acad Sci USA* 106(38):16185–16190.
62. Diensthuber RP, Bommer M, Gleichmann T, Möglich A (2013) Full-length structure of a sensor histidine kinase pinpoints coaxial coiled coils as signal transducers and modulators. *Structure* 21(7):1127–1136.
63. Casino P, Miguel-Romero L, Marina A (2014) Visualizing autophosphorylation in histidine kinases. *Nat Commun* 5:3258.
64. Kim HS, Caswell CC, Foreman R, Roop RM, 2nd, Crosson S (2013) The Brucella abortus general stress response system regulates chronic mammalian infection and is controlled by phosphorylation and proteolysis. *J Biol Chem* 288(19):13906–13916.
65. Kim HS, Willett JW, Jain-Gupta N, Fiebig A, Crosson S (2014) The Brucella abortus virulence regulator, LovhK, is a sensor kinase in the general stress response signalling pathway. *Mol Microbiol* 94(4):913–925.
66. Adams PD, et al. (2010) PHENIX: A comprehensive Python-based system for macromolecular structure solution. *Acta Crystallogr D Biol Crystallogr* 66(Pt 2):213–221.
67. Morin A, et al. (2013) Collaboration gets the most out of software. *eLife* 2:e01456.
68. Herrou J, Crosson S (2013) myo-inositol and D-ribose ligand discrimination in an ABC periplasmic binding protein. *J Bacteriol* 195(10):2379–2388.
69. Herrou J, Rotskoff G, Luo Y, Roux B, Crosson S (2012) Structural basis of a protein partner switch that regulates the general stress response of α-proteobacteria. *Proc Natl Acad Sci USA* 109(21):E1415–E1423.
70. Khan SR, Gaines J, Roop RM, 2nd, Farrand SK (2008) Broad-host-range expression vectors with tightly regulated promoters and their use to examine the influence of TraR and TraM expression on Ti plasmid quorum sensing. *Appl Environ Microbiol* 74(16):5053–5062.
71. Pronk S, et al. (2013) GROMACS 4.5: A high-throughput and highly parallel open source molecular simulation toolkit. *Bioinformatics* 29(7):845–854.
72. Lindorff-Larsen K, et al. (2010) Improved side-chain torsion potentials for the Amber ff99SB protein force field. *Proteins* 78(8):1950–1958.
73. Hess B, Bekker H, Berendsen HJC, Fraaije JGEM (1997) LINCS: A linear constraint solver for molecular simulations. *J Comput Chem* 18:1463–1472.
74. Parrinello M, Rahman A (1981) Polymorphic transitions in single crystals: A new molecular dynamics method. *J Appl Phys* 52:7182–7190.
75. Darden T, York D, Pedersen L (1993) Particle mesh Ewald: An N·log(N) method for Ewald sums in large systems. *J Chem Phys* 98:10089–10092.
76. Iancu CV, et al. (2006) Electron cryotomography sample preparation using the Vitrobot. *Nat Protoc* 1(6):2813–2819.
77. Tivol WF, Briegel A, Jensen GJ (2008) An improved cryogen for plunge freezing. *Microsc Microanal* 14(5):375–379.
78. Schneider CA, Rasband WS, Eliceiri KW (2012) NIH Image to ImageJ: 25 years of image analysis. *Nat Methods* 9(7):671–675.